
ImageAttributionBench: How Far Are We from Generalizable Attribution?

Tingshu Mou¹, Zhipeng Wei², Chao Gong¹, Jingjing Chen^{1†}, Xingjun Ma^{1†}
¹Fudan University, ²University of California, Berkeley

Abstract

The rapid advancement of generative AI has enabled the creation of highly realistic and diverse synthetic images, posing critical challenges for image provenance and misinformation detection. This underscores the urgent need for effective image attribution. However, existing attribution datasets are constrained by limited scale, outdated generation methods, and insufficient semantic diversity—hindering the development of robust and generalizable attribution models. To address these limitations, we introduce **ImageAttributionBench**, a comprehensive dataset comprising images synthesized by a wide array of advanced generative models with state-of-the-art (SOTA) architectures. Covering multiple real-world semantic domains, the dataset offers rich diversity and scale to support and accelerate progress in image attribution research. To simulate real-world attribution scenarios, we evaluate several SOTA attribution methods on ImageAttributionBench under two challenging settings: (1) training on a standard balanced split and testing on degraded images, and (2) training and testing on semantically disjoint splits. In both cases, current methods exhibit consistently poor performance, revealing significant limitations in their robustness and generalization to unseen semantic content. Our work provides a rigorous benchmark to facilitate the development and evaluation of future image attribution methods.

1 Introduction

In recent years, the emergence and evolution of auto-regressive models [18, 44, 66] and diffusion models [32, 61, 16, 50, 58, 55, 56] have led to AI-generated content (AIGC) becoming increasingly realistic and widely applied across industries, bringing convenience to fields such as entertainment [51, 2, 63], advertising [39, 17], and medicine [60, 83]. This progress is particularly evident in AI-synthesized images, which have seen gradual improvements in resolution and semantic consistency, accompanied by more accessible generation methods for users.

However, issues such as the spread of misinformation [74, 62, 81], privacy violations [48, 35], and fraud [27, 70] have become more serious. Therefore, the importance and necessity of research on traceability technologies to track the origin of synthesized images have steadily increased. This urgency has brought image attribution, also known as model attribution, to the forefront as an essential task. It involves identifying the source model of an AI-generated image—that is, determining which generative model was used to create the image.

In response to this crucial task of image attribution, several datasets have been proposed and developed over the past years to facilitate research and evaluation [80, 69, 28, 7, 78, 86]. Early image attribution datasets [80, 69] primarily use low-resolution images from single-category GAN models, covering limited GAN architectures and specific semantic domains like faces and bedrooms. Subsequent datasets [7, 78, 28, 86] expand the scale and diversity of models and images by including various GAN types, semantic categories, and the introduction of diffusion models.

[†]Corresponding author.

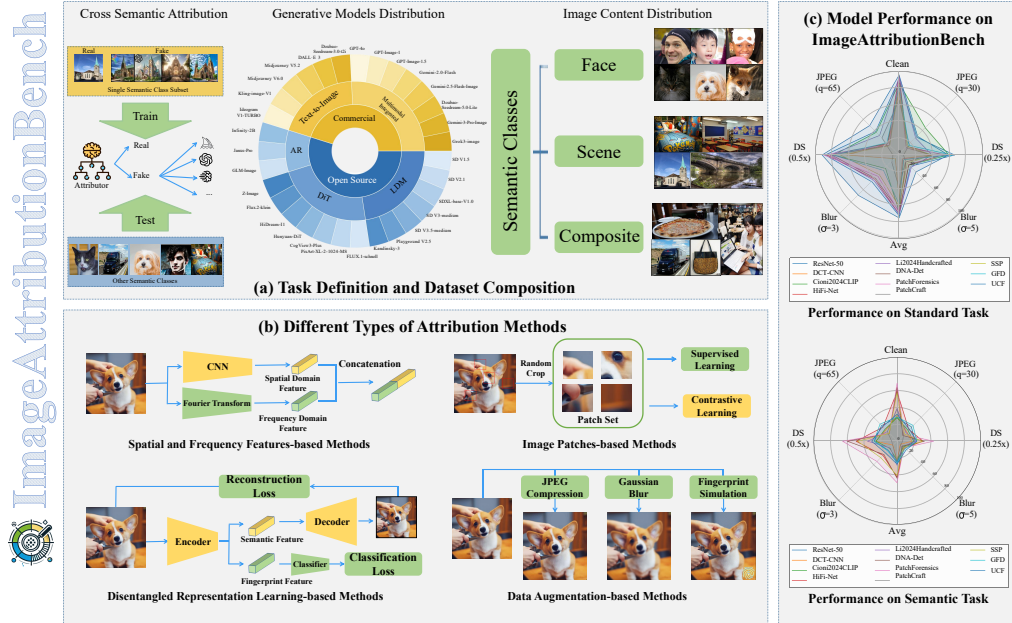


Figure 1: Overview of ImageAttributionBench. (a) The cross-semantic attribution task and key statistics of the constructed dataset. (b) Illustration of the four main categories of existing attribution methods. (c) Performance comparison of representative attributors on standard and semantic tasks under various degradations.

Despite these advancements, existing datasets suffer from critical limitations that hinder the development of robust and generalizable attribution methods: (1) **Limited Model Diversity**: The restricted number of generative models (typically ≤ 15) within these datasets inadequately reflects the complexity of real-world scenarios. (2) **Reliance on Outdated Generation Methods**: These datasets predominantly feature older GAN architectures and early diffusion models, lacking contemporary cutting-edge paradigms like Diffusion Transformers (DiT) and Auto Regressive (AR) models. (3) **Insufficient Semantic Diversity**: The limited range of semantic categories in these datasets can lead to entanglement between model-specific fingerprints and semantic features, thereby compromising the generalization capabilities of attribution models.

To address the critical limitations of existing datasets, we introduce ImageAttributionBench, a novel benchmark designed to advance the field. To better reflect the complexities of real-world image generation, ImageAttributionBench features a comprehensive suite of 31 state-of-the-art generators, comprising 17 open-sourced and 14 commercial models. Significantly, beyond conventional Latent Diffusion Models (LDM) [58], our dataset uniquely integrates cutting-edge architectures that have gained prominence in the last two years, including DiT, AR, and native multi-modal generative models. Furthermore, ImageAttributionBench introduces semantic diversity by including 10 semantic classes sourced from 6 distinct real-world datasets, thus representing a broader range of domains than previous benchmarks. ImageAttributionBench comprises roughly 640,000 images, collected from real-world datasets and synthesized using this diverse set of 31 generative models.

Table 1 provides a comparative analysis of ImageAttributionBench against existing datasets. A key design decision in our work is the exclusion of the somewhat outdated GAN architecture. It allows us to concentrate on a more extensive and varied set of advanced generative models that represent the current state of the art. Besides, the design of separate classes within datasets encourages attribution methods to capture generative-model-specific features that are independent of semantics.

To demonstrate the inherent challenges presented by ImageAttributionBench, we conduct comprehensive experiments using state-of-the-art methods from both fake image detection and attribution literature. Our evaluation encompasses two distinct settings: a standard balanced split and a more rigorous semantic-based split specifically designed to assess the generalization capabilities of these methods across diverse semantic categories. Figure 1 illustrates the overall performance of the

Table 1: Overview of existing attribution datasets. Size indicates the number of images. Models lists only neural-network generative models. Semantic Diversity indicates whether sufficient semantic classes are included. Semantic Balance indicates whether semantic distribution is balanced across generative models.

Dataset	Size	Models (by Type and Quantity)	Semantic Diversity	Semantic Balance
Yu et al. [80]	550k	4 × GAN	No	Yes
ForenSynths [69]	72k	6 × GAN	Yes	No
Attribution88 [7]	1M	7 × GAN	Yes	Yes
IFDL [28]	1.9M	4 × GAN + 4 × Diffusion	Yes	No
OSMA [78]	300k	4 × GAN	Yes	No
GenImage [86]	2.7M	1 × GAN + 7 × Diffusion	Yes	Yes
WildFake [33]	3.69M	9 × GAN + 8 × Diffusion + 4 × Other	Yes	No
WILD [6]	50k	8 × Commercial + 3 × Diffusion + 4 × DiT + 5 × Others	No	No
ours	640k	14 × Commercial + 7 × Diffusion + 7 × DiT + 3 × AR	Yes	Yes

evaluated methods on ImageAttributionBench. While all attribution methods achieve high accuracy on the standard balanced split where all semantic classes are available, their classification performance declined sharply when access is restricted to a single semantic class. This stark contrast underscores the crucial role of semantics in robust image attribution, highlighting the potential of ImageAttributionBench to drive the development of more realistic and effective attribution techniques. Our code and dataset are available at <https://github.com/mtry/ImageAttributionBench>.

2 Related Work

We categorize current image attribution methods into four key areas: spatial and frequency features, data augmentation, image patches, and disentangled representation learning. We present these methods below.

Spatial and Frequency Features-based Methods These methods exploit image statistics and high-frequency features introduced during generations for image attribution. Frank et al. [21] pioneer early work by identifying model-specific fingerprints based on Discrete Cosine Transform (DCT) spectrum artifacts. More recently, Guo et al. [28] propose HiFi-Net, a multi-branch architecture operating at different resolutions to fuse features from both color and high-frequency domains. HiFi-Net incorporates a localization module, enabling it to detect manipulated regions in CNN-synthesized or edited images. Leveraging powerful pretrained models, Cioni et al. [14] demonstrate that features extracted using CLIP, combined with a simple linear classifier, achieve state-of-the-art performance on the challenging open-world source attribution task. Building on this, Li et al. [43] combine CLIP embeddings with traditional handcrafted filter-extracted features to improve performance, particularly in small-sample training datasets.

Data Augmentation-based Methods These methods improve the generalization and robustness of the attributor by enhancing the training data. Yang et al. [77] propose DNA-Det, leveraging data augmentation through pretraining on image transformation classification combined with patch-wise contrastive learning to achieve architectural-level attribution. Subsequently, Bui et al. [7] propose a feature mixing-based augmentation strategy. Building on the idea of DNA-Det, Yang et al. [78] introduce POSE, which simulates model fingerprints using lightweight augmentation models composed of two convolutional layers.

Image Patches-based Methods These methods claim that the fingerprint traces left by models can be detected in small regions, allowing efficient attribution using only image patches. Chai et al. [9] pioneer patch-based analysis in fake image detection, using shallow networks with limited receptive fields to localize transferable local artifacts. In more recent studies, PatchCraft [85] posits that artifacts in texture-rich and texture-simple areas of generated images are inconsistent, unlike authentic images. Its approach involves segmenting images into patches and then reassembling them based on their texture complexity to facilitate fingerprint extraction. Furthermore, SSP [10] uses texture-simple

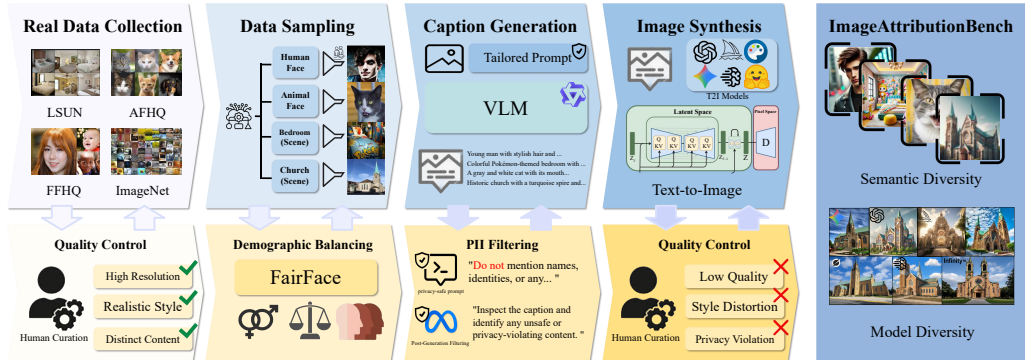


Figure 2: Pipeline of our dataset construction.

patches, which contain rich information for fingerprint extraction, because they are often neglected by generative models compared to texture-rich patches.

Disentangled Representation Learning-based Methods These methods aim to separate the forgery traces of the image from the semantic content. GFD [76] uses an encoder-decoder and an auxiliary classifier to classify real images with added fingerprints as forged, promoting fingerprint disentanglement. Building upon GFD, UCF [75] separately extracts semantic and forged features, reconstructs images from semantic features for disentanglement, using only forged for attribution.

3 Dataset Construction

The rapid advancement of generative AI necessitates a paradigm shift in image attribution research, yet existing datasets suffer from limitations in scale, outdated generation methodologies, and a critical lack of semantic diversity. To bridge this significant gap, we present ImageAttributionBench. Our dataset is designed to provide both the necessary large-scale data and the crucial semantic breadth required to effectively evaluate and advance the field. Specifically, the construction of our ImageAttributionBench dataset comprises three key steps: (1) collecting and sampling diverse real-world images from real datasets, ensuring broad coverage of visual concepts; (2) leveraging state-of-the-art large vision-language models to generate accurate and descriptive captions for these images; and (3) employing cutting-edge text-to-image models to synthesize images guided by these captions. The complete dataset construction pipeline is illustrated in Figure 2.

For each step, we employ human and AI-assisted curation to guarantee the quality and ethical integrity of our dataset. Specifically, we employ human curation during real data collection and image generation to maintain high visual quality in both real and synthesized samples. To further eliminate potential ethical concerns, we apply demographic balancing during data sampling and conduct Personally Identifiable Information (PII) filtering during caption-generation. Details of the implementation are provided in Section A of the supplemental material.

3.1 Real Data Collection

To ensure our ImageAttributionBench benefits from a broad spectrum of real-world visual concepts and semantic diversity, we initiated the dataset construction by selecting several domain-specific image datasets. These include CelebA-HQ [37] and FFHQ [38] for human faces, AFHQ [13] for animal faces, LSUN [79] for scenes, and more general ImageNet-1k [59] and COCO [46]. Specifically, for CelebA-HQ and FFHQ, we sample 2,000 images each to cover two classes of human faces. For AFHQ and LSUN, we sample 6,000 images each to cover dog, cat, wild, church, classroom, and bedroom. For ImageNet-1k, which has 1,000 labels, we sample 2 images per label, totaling 2,000 images. For COCO, we randomly sample 2,000 images. The combination of these sampling efforts results in a real-world image subset of 20,000 images spanning 10 semantic classes.

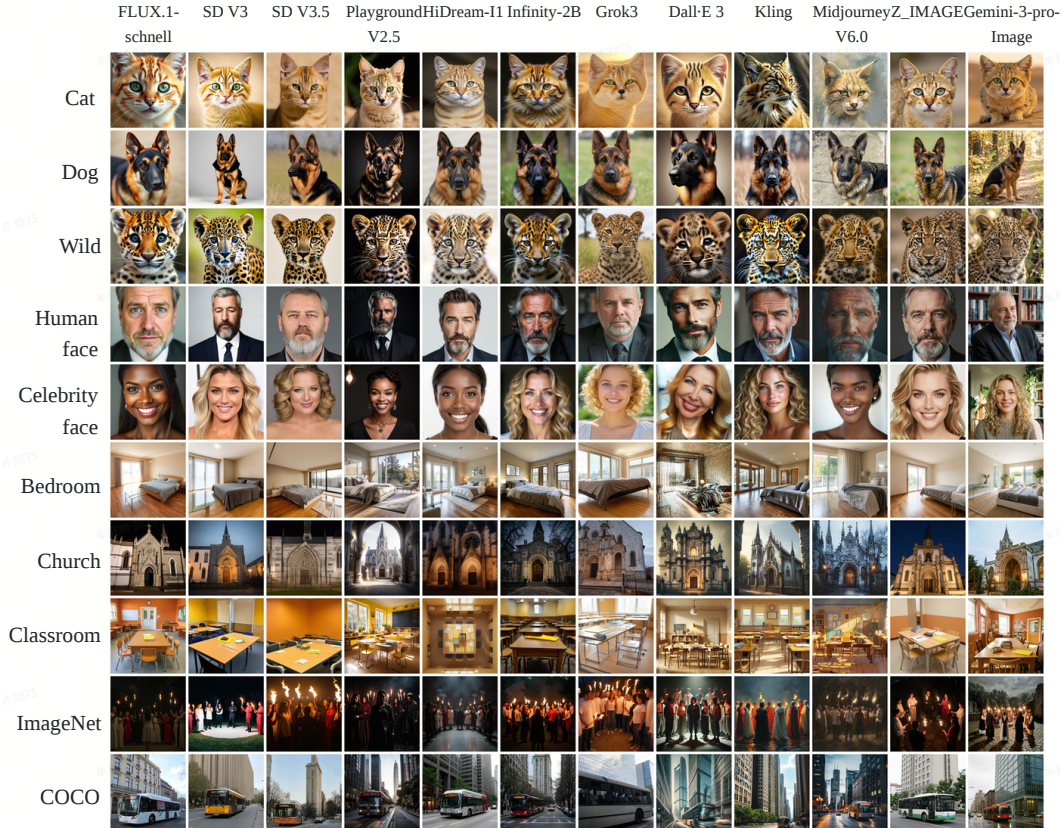


Figure 3: Visualization of images in ImageAttributionBench.

3.2 Captions Generation

To ensure the semantic fidelity of the generated captions to the original images, we utilize tailored templates for each semantic category, which then serve as prompts to guide QwenVL-chat [3] in its caption generation process. The caption templates are listed in Table 2. We design templates for all datasets to ensure that captioning focuses on the main content of each image, except for COCO, where we directly use the provided captions. To ensure consistent generation quality and to match the number of generated and real images, we select 1,000 images for each semantic class, generate 1,000 captions, and instruct each generation model to produce two images per caption. Representative image-caption pairs are provided in the supplemental material.

3.3 Image Generation

Generation Models Text-to-image generation is increasingly becoming a primary method for image creation. Therefore, we carefully selected 31 representative commercial and open-source text-to-image models widely used in real-world scenarios. The distribution of these recent generative models is shown in Figure 1.

For open-source models, we select those with relatively low video random access memory (VRAM) requirements to ensure ease of deployment on consumer-grade devices. These models span three major categories: LDM, DiT, and AR. First, LDMs include the Stable Diffusion (SD) series and other variants based on LDM paradigm. We select the following models from the SD series: SD V1.5 [57], SD V2.1 [57], SDXL-base-V1.0 [55], SD V3-medium [19], and SD V3.5-medium [19]. While SD V3 and V3.5 adopt DiT backbone, they are still widely recognized as part of the SD family. Additionally, we include other LDM-based models such as Playground V2.5 [42], and Kandinsky-3 [67]. Second, DiTs combine diffusion-based generation with transformer architectures to better capture global image context, leading to high-resolution and realistic outputs. In addition to SD V3, which follows the DiT

Table 2: Semantic classes and their corresponding prompt templates.

Semantic Class	Prompt Template
Human Face	Describe the face in the image by focusing only on general facial features. Include aspects such as the shape and appearance of the eyes, nose, mouth, and ears, the color and texture of the skin or fur, facial expression, and any visible hair or fur. Do not mention names, identities, or any personally identifiable information. The description should clearly center on the face, with minimal reference to the background or body. Keep it vivid and concise, 20 to 50 words.
Animal Face	Describe the face in the image with focus on facial features. Include details such as the shape and appearance of the eyes, nose, mouth, and ears, the color and texture of the skin or fur, facial expression, and any visible hair or fur. The description should clearly center on the face, with minimal reference to the background or body. Keep it vivid and concise, 20 to 50 words.
Scene	Describe a {scene_label} scene in the image. Focus on the main elements typical of a {scene_label}, such as objects, layout, colors, and lighting. Avoid focusing on people or irrelevant details. The description should be visual and vivid, 20 to 50 words.
ImageNet-1k	Using the given label '{label}' as guidance, describe the image in as much detail as possible, focusing on objects, setting, colors, actions, and mood. Incorporate elements related to the label. Keep the description between 20 and 50 words.

design, we also include seven representative independently developed DiT-based models: FLUX.1-schnell [41], PixArt-XL-2-1024-MS [11], CogView3-Plus [84], Hunyuan-DiT [45], HiDream-I1-fast [31], FLUX.2-klein [5], and Z-Image [65]. For simplicity, we roughly classify FLUX.2-klein as a DiT, although it is more precisely a flow-based model built around a flow transformer. Finally, AR models, which synthesize images in a token-by-token manner, have regained attention in the field due to their promising capabilities. We include three recent AR-based models: the visual text-to-image model Infinity-2B [29], the multimodal model Janus-Pro [12], and GLM-Image [82], which adopts a hybrid architecture with an AR generator and a DiT decoder.

For the commercial models, we focus on representative models with state-of-the-art performance and broad industry adoption. These can be divided into two categories: pure text-to-image generation models, including DALL·E 3 [4], Midjourney [49] (V5.2 and V6.0), Kling-image-V1 [40], Ideogram-generate-V-1-TURBO [34], and Doubao-seedream-3.0-t2i [22]; and models integrated into widely deployed large multimodal frameworks, such as GPT-4o [1], GPT-Image-1 [52], GPT-Image-1.5 [53], Gemini-2.0-Flash [23], Gemini-2.5-Flash-Image [24], Gemini-3-Pro-Image [25], Doubao-seedream-5.0-Lite [8], and Grok3-image [26].

Image Generation Finally, we use captions generated in Section 3.2 to guide these generative models for image generation. To enhance realism and ensure styles closely match those of real images, we apply negative prompts including terms such as “cartoon, anime, drawing, painting, unrealistic, deformed features, blurry, low resolution, oversaturated, illustration, flat design, vector art, 2D, simple, graphic design.” Implementation Details for generation models are as follows: for models available on Hugging Face [20], we deploy them and generate images using the Python Diffusers pipeline [68]. SD V1.5 and FLUX.1-schnell produce images at the resolution of 512×512, SD V2.1 and Kandinsky-3 at 768×768 and the rest at 1024×1024. Other open-source models are deployed via their GitHub repositories. Janus-pro generates images at 384×384, Hunyuan-DiT, Infinity-2B and HiDream-I1-fast at 1024×1024. Commercial models generate images through API calls. DALL·E 3, GPT-4o, GPT-Image-1, GPT-Image-1.5, Gemini-2.5-Flash-Image, Gemini-3-Pro-Image, Doubao-seedream-3.0-t2i, Midjourney V5.2, Midjourney V6.0, Kling-image-V1, and Ideogram-generate-V-1-TURBO all produce images at a resolution of 1024×1024. Doubao-seedream-5.0-Lite generates images at 1920×1920. Grok3-image generates images at 1024×768, and Gemini-2.0-Flash generates images at varying resolutions, with the longer side fixed at 1024.

Table 3: Comparison of different methods on both the standard balanced-split task and the semantic-split task. For the standard task, DS denotes downsampling, JPEG denotes JPEG compression, and Blur represents Gaussian blur. For the semantic task, each cell reports clean accuracy (left) and the average degraded accuracy across six degradation levels (right).

Method	Standard Task								Semantic Task			
	Clean Acc. (%)	Degraded Acc.							Training on Cat Acc.	Training on Human Face Acc.	Training on Bedroom Acc.	Avg Acc.
		DS (0.5x)	DS (0.25x)	JPEG (q=65)	JPEG (q=30)	Blur ($\sigma = 3$)	Blur ($\sigma = 5$)	Avg Acc.				
ResNet-50 [30]	89.7	89.2	83.6	77.3	60.3	58.8	<u>36.4</u>	<u>67.6</u>	21.9/19.1	26.3/23.5	18.0/14.6	22.1/19.1
DCT-CNN [21]	75.2	66.2	45.0	27.7	20.1	6.0	1.2	27.7	23.2/13.7	34.0/15.9	30.9/15.2	29.4/14.9
HiFi-Net [28]	96.8	88.9	60.1	16.0	13.5	36.7	10.2	37.6	50.8/24.8	61.9/24.0	56.4/25.6	56.4/24.8
Li et al. [43]	96.6	89.5	65.0	40.0	36.0	47.1	11.8	48.2	44.9/19.3	51.1/20.2	43.2/17.6	46.4/19.0
DNA-Det [77]	92.9	87.2	56.4	14.8	12.9	44.7	12.1	38.0	<u>68.6/28.5</u>	74.6/26.4	<u>70.6/27.1</u>	71.3/27.3
RepMix [7]	90.0	89.2	<u>80.2</u>	<u>89.8</u>	<u>81.0</u>	37.3	19.0	66.1	66.3/ 50.3	59.9/ 49.1	66.6/ 48.8	64.3/ 49.4
PatchForensics [9]	93.8	89.2	60.2	14.6	12.2	44.2	10.2	38.4	69.1/32.6	<u>67.2/29.7</u>	73.4/35.1	<u>69.9/32.5</u>
PatchCraft [85]	73.5	5.3	3.9	32.9	13.1	8.7	7.2	11.9	44.5/8.4	39.0/8.1	39.1/7.1	40.9/7.9
SSP [10]	89.0	76.5	39.3	12.7	7.7	43.4	15.1	32.5	61.2/24.9	62.0/23.5	61.3/24.2	61.5/24.2
GFD [76]	87.7	79.8	53.5	70.9	44.7	13.4	4.7	44.5	45.9/ <u>34.0</u>	25.7/22.3	43.0/25.7	37.2/27.3
UCF [75]	95.9	94.0	75.2	40.4	24.3	43.3	9.0	47.7	16.9/13.5	21.8/17.6	17.9/12.4	18.9/14.5
FSD [73]	97.5	<u>95.5</u>	71.5	62.4	62.4	<u>68.1</u>	26.6	64.4	35.3/23.6	36.8/21.4	34.3/20.3	35.5/21.7
Omni-DFA [72]	<u>97.2</u>	96.4	79.0	96.1	83.8	95.6	89.0	90.0	36.5/29.1	43.4/ <u>35.7</u>	39.5/29.6	39.8/31.5
Avg	90.4	80.5	59.5	45.8	36.3	42.1	19.4	47.3	45.0/24.7	45.8/24.5	46.1/23.2	45.6/24.2

Sample generated images are shown in Figure 3, where the vertical axis indicates the semantic classes, and the horizontal axis corresponds to a subset of generative models used in our dataset construction. Additional visualizations are provided in Section G of the supplemental material.

4 Experimental Setup

Attribution Methods As we mention in Section 2, existing methods can be categorized into four classes. For each class, we select a few representative methods. For the spatial and frequency feature-based methods, we select ResNet-50 [30] pretrained on ImageNet [59]; DCT-CNN [21], which exploits the frequency domain; the method from [14], which utilizes a CLIP model for feature extraction and a logistic regressor for classification; and HiFi-Net [28] (without the localization module, since it is not applicable to this task). We also reproduce method from [43], which employs a handcrafted filter combined with the CLIP feature extractor. To obtain better and more stable results, we replace the reference set average distance classifier with a neural network classifier. For the data augmentation-based methods, we choose DNA-Det [77] with two phases of training and RepMix [7]. For the image patch-based methods, we leverage PatchForensics [9], SSP [10], and reproduce PatchCraft [85]. For the disentangled representation learning-based methods, we reproduce GFD [76] and adapt UCF [75] from a detection task to an attribution task. We also incorporate two SOTA few-shot detectors, FSD [73] and Omni-DFA [72], and tailor them to the attribution task.

Evaluation Settings We evaluate these methods in two tasks: a standard balanced-split task and a semantic-split task. For the standard balanced-split task, we typically divide the dataset into three subsets: training, validation and testing, with a ratio of 8:1:1. We balance the labels to ensure an equal distribution across all classes. For the semantic-split task, the train-validation and test sets are split based on semantic classes. Specifically, the training and validation sets contain samples from only one semantic class, split in a 9:1 ratio, while the test set consists of samples from the remaining classes. This kind of split significantly reduces the utilization of semantic information and challenges the capability to extract semantic-irrelevant fingerprints of generative models. For this task, we design three sub-tasks that use cat faces from AFHQ, human faces from FFHQ, and bedrooms from LSUN for training and validation, respectively. In real-world scenarios, images often undergo various types of degradation, such as compression, cropping, and blurring during transmission across social media platforms. Therefore, to simulate these conditions and evaluate the robustness of each attributor, we apply six degradation levels that include various types—downsampling, JPEG compression, and Gaussian blur—with different intensities, following the protocol in GenImage [86]. Regarding metrics, we use accuracy to measure the performance. During evaluation, we resize and center-crop images to 256×256 and train each attributor equally for 10 epochs on the standard task and 15 epochs on the semantic task, ensuring that all can fit on the training set. We then select the best checkpoint based on validation set performance and evaluate on the test set.

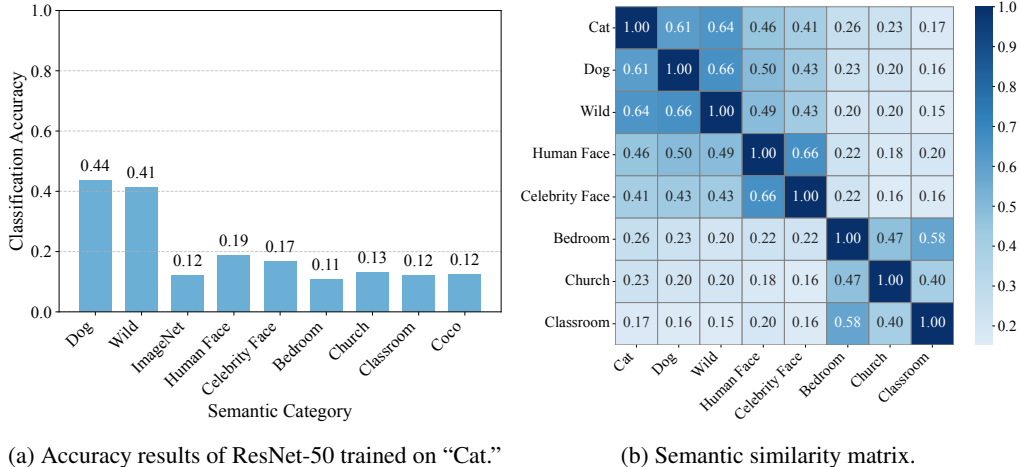


Figure 4: Performance of ResNet-50 and semantic similarity matrix. (a) Accuracy results for each semantic category obtained from ResNet-50 trained on "Cat." (b) Semantic similarity matrix across different subsets.

5 Results

In this section, we discuss the performances of SOTA attributors on ImageAttributionBench. We review the results on standard split task with both clean and degraded testing data. Furthermore, we evaluate performance on semantic-split task, and analyze the correlation between accuracy and semantic similarity of the training and testing subsets.

Performance on Standard Balanced-Split Task Following evaluation settings in Section 4, we first conduct experiments on the standard task, and results are shown in the left half of Table 3. On clean images, most attributors exceed 80%, with an average accuracy of 90.4%. Notably, FSD, originally proposed for few-shot fake image detection, attains the highest performance at 97.5%, while even the pretrained ResNet-50 reaches 89.7%. This indicates that the availability of full semantic information in the standard task simplifies the attribution process.

However, under the more practical scenario of image degradation, the average accuracy of all attributors drops sharply from 90.4% to 47.3%. This indicates that the degradation of spatial details, frequency structures, and edge information poses a considerable challenge for current attributors. In contrast, superior methods like Omni-DFA and RepMix use data augmentation in data processing or leverage feature-mixing strategies, leading to better performance under such conditions. This underscores the importance of developing more robust feature extraction techniques to handle image degradation effectively.

Performance on Semantic-Split Task In the semantic task, the dataset is divided into 10 semantically distinct subsets (e.g., "Cat", "Human face", "Bedroom"). We then perform training on one subset at a time and evaluate these methods on the remaining nine. The results of this evaluation are presented in the right half of Table 3. Compared to the standard task, the semantic task results in a significant drop in clean average performance, from 90.4% to around 45.6%. Notably, the best-performing methods on the standard task, FSD and Omni-DFA, yield poor performance on the semantic task, with accuracies below 40%, exhibiting significant performance drops of over 50 percentage points. This suggests that the separation of semantic categories can have a similarly detrimental effect on performance as image degradation. DNA-Det and RepMix show comparatively strong performance on the semantic task. This highlights that data augmentations, such as feature mixing and pretraining with image transformations, can improve generalization ability even when the model is trained on images from a single semantic category. Despite this robustness, DNA-Det and RepMix still experience clear performance declines of 21.6 and 25.7 percentage points, respectively, from the standard clean task to the semantic clean task. PatchForensics and SSP achieve moderately high accuracy, demonstrating the potential of local patch information in cross-semantic attribution. In contrast, PatchCraft does not achieve similar results, as its strategy is specifically designed for

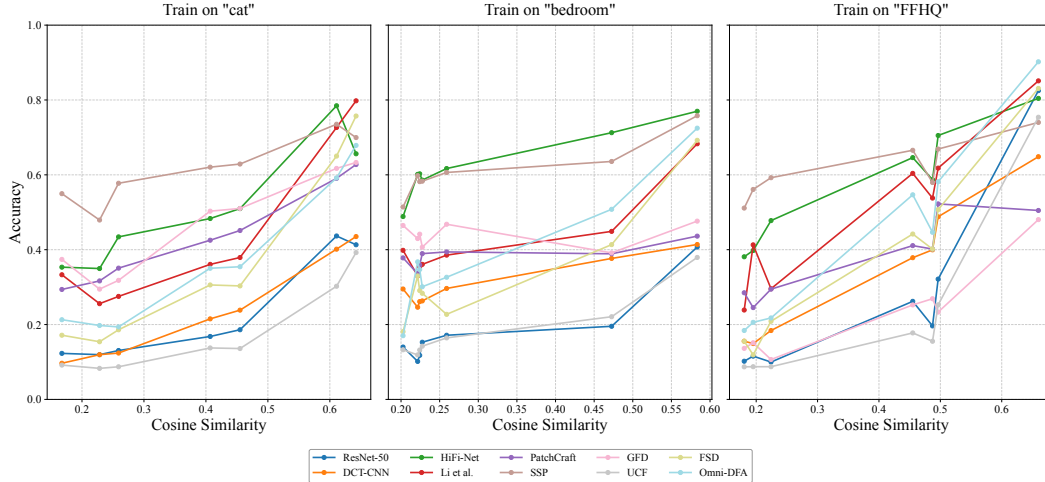


Figure 5: Accuracy against semantic similarity for different attribution models across various training settings, i.e., training on “cat”, “bedroom”, and “FFHQ”.

detection rather than attribution. Under image degradation, the semantic task shows a further 21.4% drop in average performance, from 45.6% to 24.2%. This highlights that existing attribution methods still have significant room for improvement in more challenging yet practical scenarios.

Correlation Between Accuracy and Semantic Similarity To investigate the relationship between attribution accuracy and semantic similarity, we report per-subset accuracy in Figure 4a using ResNet-50 trained on the “cat” category, and show the category similarity matrix in Figure 4b, where 100 randomly selected captions are encoded into sentence embeddings and their cluster centers compared using cosine similarity. From these results, we observe that attribution accuracy declines as the semantic similarity to the training category “cat” decreases. For instance, “dog” and “wild” categories, which are semantically close to “cat”, achieve relatively high accuracy. To further illustrate this relationship more explicitly, we plot accuracy against similarity across various training settings in Figure 5. As shown, there is a clear positive correlation between accuracy and semantic similarity. This suggests that existing methods benefit from semantic correlations between training and testing splits in current datasets. Therefore, semantic separation in ImageAttributionBench is crucial for a more rigorous and realistic evaluation of attribution performance.

6 Limitations

Our proposed ImageAttributionBench introduces a novel resource encompassing state-of-the-art generative model architectures and presents challenges to attribution tasks. While acknowledging that our initial release is not exhaustive, we have focused on establishing a strong foundation. Specifically, our semantic coverage includes several commonly studied categories in attribution, providing a targeted benchmark for current research. Similarly, we have adopted a photorealistic style to align with real-world imagery. Recognizing the resource constraints of initial data generation, we provide 2,000 high-quality images per model per semantic category, offering a substantial dataset for practical evaluation. We envision significant potential for future extensions, including incorporation of a broader spectrum of semantic categories (e.g., drawing inspiration from the diversity of ImageNet), exploration of artistic and other stylistic variations, and scaling to larger dataset sizes to facilitate more comprehensive analyses of attribution methods.

7 Conclusion

This paper introduces ImageAttributionBench, a benchmark specialized for AI-synthesized image attribution. ImageAttributionBench surpasses previous datasets in both the number and advancement of generative model architectures it includes, while maintaining semantic diversity and balance

across models. We conduct two main experiments on ImageAttributionBench, namely the standard balanced-split task and the semantic-split task, and the results demonstrate the limitations of existing attribution methods in terms of robustness to degradation and semantic generalization. Additionally, we provide a quantitative analysis of the correlation between accuracy and semantic similarity, showing the need for improved attribution methods to overcome semantic entanglement. We hope that ImageAttributionBench will inspire the AI community to advance attribution techniques that are robust, semantically generalizable, and applicable in real-world settings.

References

- [1] Josh Achiam, Steven Adler, Sandhini Agarwal, Lama Ahmad, Ilge Akkaya, Florencia Leoni Aleman, Diogo Almeida, Janko Altenschmidt, Sam Altman, Shyamal Anadkat, et al. Gpt-4 technical report. *arXiv preprint arXiv:2303.08774*, 2023.
- [2] AI Dungeon. Ai dungeon: Ai-powered text adventure game. <https://aidungeon.com/>.
- [3] Jinze Bai, Shuai Bai, Shusheng Yang, Shijie Wang, Sinan Tan, Peng Wang, Junyang Lin, Chang Zhou, and Jingren Zhou. Qwen-vl: A versatile vision-language model for understanding, localization, text reading, and beyond. *arXiv preprint arXiv:2308.12966*, 2023.
- [4] James Betker, Gabriel Goh, Li Jing, Tim Brooks, Jianfeng Wang, Linjie Li, Long Ouyang, Juntang Zhuang, Joyce Lee, Yufei Guo, et al. Improving image generation with better captions. *Computer Science*. <https://cdn.openai.com/papers/dall-e-3.pdf>, 2(3):8, 2023.
- [5] Black Forest Labs. FLUX.2 [klein]: Towards interactive visual intelligence, January 2026. URL <https://bf1.ai/blog/flux2-klein-towards-interactive-visual-intelligence>.
- [6] Pietro Bongini, Sara Mandelli, Andrea Montibeller, Mirko Casu, Orazio Pontorno, Claudio Vittorio Ragaglia, Luca Zanchetta, Mattia Aquilina, Taiba Majid Wani, Luca Guarnera, et al. Wild: a new in-the-wild image linkage dataset for synthetic image attribution. In *2025 International Joint Conference on Neural Networks (IJCNN)*, pages 1–8. IEEE, 2025.
- [7] Tu Bui, Ning Yu, and John Collomosse. Repmix: Representation mixing for robust attribution of synthesized images. In *European Conference on Computer Vision*, pages 146–163. Springer, 2022.
- [8] ByteDance Seed Team. Deeper thinking, more accurate generation: Introducing Seedream 5.0 lite, February 2026. URL <https://seed.bytedance.com/en/blog/deeper-thinking-more-accurate-generation-introducing-seedream-5-0-lite>.
- [9] Lucy Chai, David Bau, Ser-Nam Lim, and Phillip Isola. What makes fake images detectable? understanding properties that generalize. In *Computer vision—ECCV 2020: 16th European conference, Glasgow, UK, August 23–28, 2020, proceedings, part XXVI 16*, pages 103–120. Springer, 2020.
- [10] Jiaxuan Chen, Jieteng Yao, and Li Niu. A single simple patch is all you need for ai-generated image detection. *arXiv preprint arXiv:2402.01123*, 2024.
- [11] Junsong Chen, Jincheng Yu, Chongjian Ge, Lewei Yao, Enze Xie, Yue Wu, Zhongdao Wang, James Kwok, Ping Luo, Huchuan Lu, et al. Pixart- α : Fast training of diffusion transformer for photorealistic text-to-image synthesis. *arXiv preprint arXiv:2310.00426*, 2023.
- [12] Xiaokang Chen, Zhiyu Wu, Xingchao Liu, Zizheng Pan, Wen Liu, Zhenda Xie, Xingkai Yu, and Chong Ruan. Janus-pro: Unified multimodal understanding and generation with data and model scaling. *arXiv preprint arXiv:2501.17811*, 2025.
- [13] Yunjey Choi, Youngjung Uh, Jaejun Yoo, and Jung-Woo Ha. Stargan v2: Diverse image synthesis for multiple domains. In *Proceedings of the IEEE/CVF conference on computer vision and pattern recognition*, pages 8188–8197, 2020.
- [14] Dario Cioni, Christos Tzelepis, Lorenzo Seidenari, and Ioannis Patras. Are clip features all you need for universal synthetic image origin attribution? *arXiv preprint arXiv:2408.09153*, 2024.
- [15] Riccardo Corvi, Davide Cozzolino, Giada Zingarini, Giovanni Poggi, Koki Nagano, and Luisa Verdoliva. On the detection of synthetic images generated by diffusion models. In *ICASSP 2023-2023 IEEE International Conference on Acoustics, Speech and Signal Processing (ICASSP)*, pages 1–5. IEEE, 2023.
- [16] Prafulla Dhariwal and Alexander Nichol. Diffusion models beat gans on image synthesis. *Advances in neural information processing systems*, 34:8780–8794, 2021.

- [17] Duo Du, Yanling Zhang, and Jiao Ge. Effect of ai generated content advertising on consumer engagement. In *International conference on human-computer interaction*, pages 121–129. Springer, 2023.
- [18] Patrick Esser, Robin Rombach, and Bjorn Ommer. Taming transformers for high-resolution image synthesis. In *Proceedings of the IEEE/CVF conference on computer vision and pattern recognition*, pages 12873–12883, 2021.
- [19] Patrick Esser, Sumith Kulal, Andreas Blattmann, Rahim Entezari, Jonas Müller, Harry Saini, Yam Levi, Dominik Lorenz, Axel Sauer, Frederic Boesel, et al. Scaling rectified flow transformers for high-resolution image synthesis. In *Forty-first international conference on machine learning*, 2024.
- [20] Hugging Face. Hugging face. <https://huggingface.co/>.
- [21] Joel Frank, Thorsten Eisenhofer, Lea Schönherr, Asja Fischer, Dorothea Kolossa, and Thorsten Holz. Leveraging frequency analysis for deep fake image recognition. In *International conference on machine learning*, pages 3247–3258. PMLR, 2020.
- [22] Yu Gao, Lixue Gong, Qiushan Guo, Xiaoxia Hou, Zhichao Lai, Fanshi Li, Liang Li, Xiaochen Lian, Chao Liao, Liyang Liu, et al. Seedream 3.0 technical report. *arXiv preprint arXiv:2504.11346*, 2025.
- [23] gemini. <https://aistudio.google.com/>, 2025.
- [24] Google Cloud. Gemini 2.5 flash image, October 2025. URL <https://docs.cloud.google.com/vertex-ai/generative-ai/docs/models/gemini/2-5-flash-image>.
- [25] Google Cloud. Gemini 3 pro image, November 2025. URL <https://docs.cloud.google.com/vertex-ai/generative-ai/docs/models/gemini/3-pro-image>.
- [26] grok3. <https://grok.com/>, 2025.
- [27] Danhui Guo, Huixuan Chen, Ruoling Wu, and Yangang Wang. Aigc challenges and opportunities related to public safety: a case study of chatgpt. *Journal of Safety Science and Resilience*, 4(4):329–339, 2023.
- [28] Xiao Guo, Xiaohong Liu, Zhiyuan Ren, Steven Grosz, Iacopo Masi, and Xiaoming Liu. Hierarchical fine-grained image forgery detection and localization. In *Proceedings of the IEEE/CVF Conference on Computer Vision and Pattern Recognition*, pages 3155–3165, 2023.
- [29] Jian Han, Jinlai Liu, Yi Jiang, Bin Yan, Yuqi Zhang, Zehuan Yuan, Bingyue Peng, and Xiaobing Liu. Infinity: Scaling bitwise autoregressive modeling for high-resolution image synthesis, 2024. URL <https://arxiv.org/abs/2412.04431>.
- [30] Kaiming He, Xiangyu Zhang, Shaoqing Ren, and Jian Sun. Deep residual learning for image recognition. In *Proceedings of the IEEE conference on computer vision and pattern recognition*, pages 770–778, 2016.
- [31] HiDream-ai. hidream-11-fast Model on Huggingface. <https://huggingface.co/HiDream-ai/HiDream-11-Fast>, 2025. Accessed: 2025-04-25.
- [32] Jonathan Ho, Ajay Jain, and Pieter Abbeel. Denoising diffusion probabilistic models. *Advances in neural information processing systems*, 33:6840–6851, 2020.
- [33] Yan Hong and Jianfu Zhang. Wildfake: A large-scale challenging dataset for ai-generated images detection. *arXiv preprint arXiv:2402.11843*, 2024.
- [34] ideogram. <https://ideogram.ai>, 2023.
- [35] Ginger Zhe Jin et al. *Artificial intelligence and consumer privacy*. Number w24253. National Bureau of Economic Research, 2018.
- [36] Kimmo Karkkainen and Jungseock Joo. Fairface: Face attribute dataset for balanced race, gender, and age for bias measurement and mitigation. In *Proceedings of the IEEE/CVF Winter Conference on Applications of Computer Vision*, pages 1548–1558, 2021.
- [37] Tero Karras, Timo Aila, Samuli Laine, and Jaakko Lehtinen. Progressive growing of gans for improved quality, stability, and variation. *arXiv preprint arXiv:1710.10196*, 2017.
- [38] Tero Karras, Samuli Laine, and Timo Aila. A style-based generator architecture for generative adversarial networks. In *Proceedings of the IEEE/CVF conference on computer vision and pattern recognition*, pages 4401–4410, 2019.

- [39] Jan Kietzmann, Jeannette Paschen, and Emily Treen. Artificial intelligence in advertising: How marketers can leverage artificial intelligence along the consumer journey. *Journal of Advertising Research*, 58(3): 263–267, 2018.
- [40] kling. <https://klingai.com/cn/dev/model/image>, 2024.
- [41] Black Forest Labs. Flux. <https://github.com/black-forest-labs/flux>, 2024.
- [42] Daiqing Li, Aleks Kamko, Ehsan Akhgari, Ali Sabet, Linmiao Xu, and Suhail Doshi. Playground v2.5: Three insights towards enhancing aesthetic quality in text-to-image generation, 2024.
- [43] Jialiang Li, Haoyue Wang, Sheng Li, Zhenxing Qian, Xinpeng Zhang, and Athanasios V Vasilakos. Are handcrafted filters helpful for attributing ai-generated images? In *Proceedings of the 32nd ACM International Conference on Multimedia*, pages 10698–10706, 2024.
- [44] Tianhong Li, Yonglong Tian, He Li, Mingyang Deng, and Kaiming He. Autoregressive image generation without vector quantization. *Advances in Neural Information Processing Systems*, 37:56424–56445, 2024.
- [45] Zhimin Li, Jianwei Zhang, Qin Lin, Jiangfeng Xiong, Yanxin Long, Xinchi Deng, Yingfang Zhang, Xingchao Liu, Minbin Huang, Zedong Xiao, Dayou Chen, Jiajun He, Jiahao Li, Wenyue Li, Chen Zhang, Rongwei Quan, Jianxiang Lu, Jiabin Huang, Xiaoyan Yuan, Xiaoxiao Zheng, Yixuan Li, Jihong Zhang, Chao Zhang, Meng Chen, Jie Liu, Zheng Fang, Weiyang Wang, Jinbao Xue, Yangyu Tao, Jianchen Zhu, Kai Liu, Sihuan Lin, Yifu Sun, Yun Li, Dongdong Wang, Mingtao Chen, Zhichao Hu, Xiao Xiao, Yan Chen, Yuhong Liu, Wei Liu, Di Wang, Yong Yang, Jie Jiang, and Qinglin Lu. Hunyuan-dit: A powerful multi-resolution diffusion transformer with fine-grained chinese understanding, 2024.
- [46] Tsung-Yi Lin, Michael Maire, Serge Belongie, James Hays, Pietro Perona, Deva Ramanan, Piotr Dollár, and C Lawrence Zitnick. Microsoft coco: Common objects in context. In *Computer vision—ECCV 2014: 13th European conference, zurich, Switzerland, September 6–12, 2014, proceedings, part v 13*, pages 740–755. Springer, 2014.
- [47] Dong C Liu and Jorge Nocedal. On the limited memory bfgs method for large scale optimization. *Mathematical programming*, 45(1):503–528, 1989.
- [48] Karl Manheim and Lyric Kaplan. Artificial intelligence: Risks to privacy and democracy. *Yale JL & Tech.*, 21:106, 2019.
- [49] Midjourney. <https://www.midjourney.com/home/>, 2022.
- [50] Alex Nichol, Prafulla Dhariwal, Aditya Ramesh, Pranav Shyam, Pamela Mishkin, Bob McGrew, Ilya Sutskever, and Mark Chen. Glide: Towards photorealistic image generation and editing with text-guided diffusion models. *arXiv preprint arXiv:2112.10741*, 2021.
- [51] OpenAI. Sora: Openai’s ai-powered text ui. <https://openai.com/sora/>.
- [52] OpenAI. Introducing our latest image generation model in the API, April 2025. URL <https://openai.com/index/image-generation-api/>.
- [53] OpenAI. The new ChatGPT images is here, December 2025. URL <https://openai.com/index/new-chatgpt-images-is-here/>.
- [54] David Patterson, Joseph Gonzalez, Urs Hölzle, Quoc Le, Chen Liang, Lluís-Miquel Munguia, Daniel Rothchild, David R So, Maud Texier, and Jeff Dean. The carbon footprint of machine learning training will plateau, then shrink. *Computer*, 55(7):18–28, 2022.
- [55] Dustin Podell, Zion English, Kyle Lacey, Andreas Blattmann, Tim Dockhorn, Jonas Müller, Joe Penna, and Robin Rombach. Sd-xl: Improving latent diffusion models for high-resolution image synthesis. *arXiv preprint arXiv:2307.01952*, 2023.
- [56] Aditya Ramesh, Prafulla Dhariwal, Alex Nichol, Casey Chu, and Mark Chen. Hierarchical text-conditional image generation with clip latents. *arXiv preprint arXiv:2204.06125*, 1(2):3, 2022.
- [57] Robin Rombach, Andreas Blattmann, Dominik Lorenz, Patrick Esser, and Björn Ommer. High-resolution image synthesis with latent diffusion models. In *Proceedings of the IEEE/CVF Conference on Computer Vision and Pattern Recognition (CVPR)*, pages 10684–10695, June 2022.
- [58] Robin Rombach, Andreas Blattmann, Dominik Lorenz, Patrick Esser, and Björn Ommer. High-resolution image synthesis with latent diffusion models. In *Proceedings of the IEEE/CVF conference on computer vision and pattern recognition*, pages 10684–10695, 2022.

- [59] Olga Russakovsky, Jia Deng, Hao Su, Jonathan Krause, Sanjeev Satheesh, Sean Ma, Zhiheng Huang, Andrej Karpathy, Aditya Khosla, Michael Bernstein, Alexander C. Berg, and Li Fei-Fei. ImageNet Large Scale Visual Recognition Challenge. *International Journal of Computer Vision (IJCV)*, 115(3):211–252, 2015. doi: 10.1007/s11263-015-0816-y.
- [60] Liangjing Shao, Benshuang Chen, Ziqun Zhang, Zhen Zhang, and Xinrong Chen. Artificial intelligence generated content (aigc) in medicine: A narrative review. *Mathematical Biosciences and Engineering*, 21(1):1672–1711, 2024.
- [61] Jiaming Song, Chenlin Meng, and Stefano Ermon. Denoising diffusion implicit models. *arXiv preprint arXiv:2010.02502*, 2020.
- [62] LI Sophia. The social harms of ai-generated fake news: Addressing deepfake and ai political manipulation. *Digital Society & Virtual Governance*, 1(1):72–88, 2025.
- [63] Sudowrite. Sudowrite: Ai writing partner. <https://sudowrite.com/>.
- [64] Qwen Team. Qwen2.5-vl, January 2025. URL <https://qwenlm.github.io/blog/qwen2.5-vl/>.
- [65] Z-Image Team. Z-image: An efficient image generation foundation model with single-stream diffusion transformer. *arXiv preprint arXiv:2511.22699*, 2025.
- [66] Keyu Tian, Yi Jiang, Zehuan Yuan, Bingyue Peng, and Liwei Wang. Visual autoregressive modeling: Scalable image generation via next-scale prediction. *Advances in neural information processing systems*, 37:84839–84865, 2024.
- [67] Arkhipkin Vladimir, Viacheslav Vasilev, Andrei Filatov, Igor Pavlov, Julia Agafonova, Nikolai Gerasimenko, Anna Averchenkova, Evelina Mironova, Bukashkin Anton, Konstantin Kulikov, Andrey Kuznetsov, and Denis Dimitrov. Kandinsky 3: Text-to-image synthesis for multifunctional generative framework. In Delia Irazu Hernandez Farias, Tom Hope, and Manling Li, editors, *Proceedings of the 2024 Conference on Empirical Methods in Natural Language Processing: System Demonstrations*, pages 475–485, Miami, Florida, USA, November 2024. Association for Computational Linguistics. URL <https://aclanthology.org/2024.emnlp-demo.48>.
- [68] Patrick von Platen, Suraj Patil, Anton Lozhkov, Pedro Cuenca, Nathan Lambert, Kashif Rasul, Mishig Davaadorj, Dhruv Nair, Sayak Paul, William Berman, Yiyi Xu, Steven Liu, and Thomas Wolf. Diffusers: State-of-the-art diffusion models. <https://github.com/huggingface/diffusers>, 2022.
- [69] Sheng-Yu Wang, Oliver Wang, Richard Zhang, Andrew Owens, and Alexei A Efros. Cnn-generated images are surprisingly easy to spot... for now. In *Proceedings of the IEEE/CVF conference on computer vision and pattern recognition*, pages 8695–8704, 2020.
- [70] TY Wang, Li Li, Xiang Chen, and KZ Li. A study on the risks and countermeasures of false information caused by aigc. *Journal of Electrical Systems*, 20(3):420–426, 2024.
- [71] Weiyun Wang, Zhangwei Gao, Lixin Gu, Hengjun Pu, Long Cui, Xingguang Wei, Zhaoyang Liu, Linglin Jing, Shenglong Ye, Jie Shao, et al. Internvl3.5: Advancing open-source multimodal models in versatility, reasoning, and efficiency. *arXiv preprint arXiv:2508.18265*, 2025.
- [72] Shiyu Wu, Shuyan Li, Jing Li, Jing Liu, and Yequan Wang. Omnidfa: A unified framework for open set synthesis image detection and few-shot attribution, 2025. URL <https://arxiv.org/abs/2509.25682>.
- [73] Shiyu Wu, Jing Liu, Jing Li, and Yequan Wang. Few-shot learner generalizes across ai-generated image detection, 2025. URL <https://arxiv.org/abs/2501.08763>.
- [74] Danni Xu, Shaojing Fan, and Mohan Kankanhalli. Combating misinformation in the era of generative ai models. In *Proceedings of the 31st ACM International Conference on Multimedia*, pages 9291–9298, 2023.
- [75] Zhiyuan Yan, Yong Zhang, Yanbo Fan, and Baoyuan Wu. Ucf: Uncovering common features for generalizable deepfake detection. In *Proceedings of the IEEE/CVF International Conference on Computer Vision*, pages 22412–22423, 2023.
- [76] Tianyun Yang, Juan Cao, Qiang Sheng, Lei Li, Jiaqi Ji, Xirong Li, and Sheng Tang. Learning to disentangle gan fingerprint for fake image attribution. *arXiv preprint arXiv:2106.08749*, 2021.
- [77] Tianyun Yang, Ziyao Huang, Juan Cao, Lei Li, and Xirong Li. Deepfake network architecture attribution. In *Proceedings of the AAAI Conference on Artificial Intelligence*, volume 36, pages 4662–4670, 2022.

- [78] Tianyun Yang, Danding Wang, Fan Tang, Xinying Zhao, Juan Cao, and Sheng Tang. Progressive open space expansion for open-set model attribution. In *Proceedings of the IEEE/CVF Conference on Computer Vision and Pattern Recognition*, pages 15856–15865, 2023.
- [79] Fisher Yu, Yinda Zhang, Shuran Song, Ari Seff, and Jianxiong Xiao. Lsun: Construction of a large-scale image dataset using deep learning with humans in the loop. *arXiv preprint arXiv:1506.03365*, 2015.
- [80] Ning Yu, Larry S Davis, and Mario Fritz. Attributing fake images to gans: Learning and analyzing gan fingerprints. In *Proceedings of the IEEE/CVF international conference on computer vision*, pages 7556–7566, 2019.
- [81] Xiaomin Yu, Yezhaohui Wang, Yanfang Chen, Zhen Tao, Dinghao Xi, Shichao Song, Simin Niu, and Zhiyu Li. Fake artificial intelligence generated contents (faigc): A survey of theories, detection methods, and opportunities. *arXiv preprint arXiv:2405.00711*, 2024.
- [82] Z.ai Team. GLM-image: Auto-regressive for dense-knowledge and high-fidelity image generation, January 2026. URL <https://z.ai/blog/glm-image>.
- [83] Peng Zhang and Maged N Kamel Boulos. Generative ai in medicine and healthcare: promises, opportunities and challenges. *Future Internet*, 15(9):286, 2023.
- [84] Wendi Zheng, Jiayan Teng, Zhuoyi Yang, Weihang Wang, Jidong Chen, Xiaotao Gu, Yuxiao Dong, Ming Ding, and Jie Tang. Cogview3: Finer and faster text-to-image generation via relay diffusion. *arXiv preprint arXiv:2403.05121*, 2024.
- [85] Nan Zhong, Yiran Xu, Sheng Li, Zhenxing Qian, and Xinpeng Zhang. Patchcraft: Exploring texture patch for efficient ai-generated image detection. *arXiv preprint arXiv:2311.12397*, 2023.
- [86] Mingjian Zhu, Hanting Chen, Qiangyu Yan, Xudong Huang, Guanyu Lin, Wei Li, Zhijun Tu, Hailin Hu, Jie Hu, and Yunhe Wang. Genimage: A million-scale benchmark for detecting ai-generated image. *Advances in Neural Information Processing Systems*, 36:77771–77782, 2023.

Table 4: Text and image similarity of different VLMs with QwenVL-Chat. Text similarity is measured using Sentence-BERT similarity, while image similarity is measured using CLIP similarity.

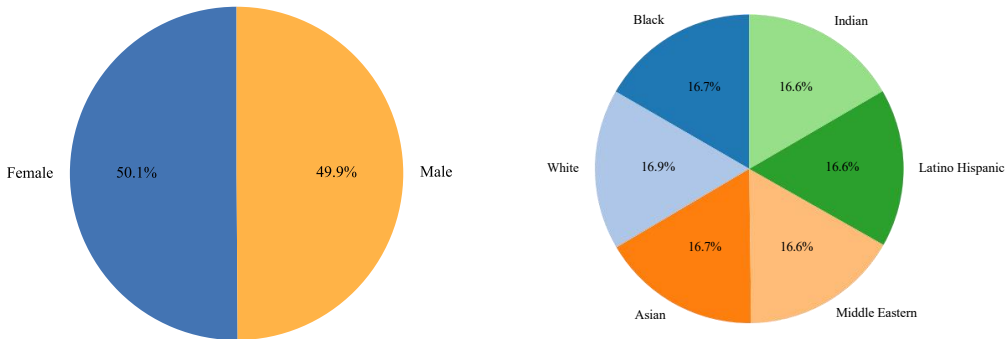
Model	Text Similarity	Image Similarity
Qwen2.5-VL-7B [64]	0.7521	0.9704
Llama-3.2-11B-Vision-Instruct [54]	0.7390	0.9813
InternVL3-8B [71]	0.7388	0.9756

A Ethical Data Curation and Protection

Given the inclusion of human faces in our dataset, we take the ethical considerations surrounding face-related images seriously. To address these issues, we apply demographic balancing during data sampling and perform Personally Identifiable Information (PII) filtering in caption generation.

For demographic balancing, we make every effort to ensure fair gender and race representation within the dataset. To achieve this, we employ FairFace [36], a gender and race detector, to sample a representative subset of real images (e.g., FFHQ and CelebA-HQ) with balanced gender and racial distributions. The resulting demographic distribution is illustrated in Figure 6.

For PII filtering, we design privacy-safe prompts for human face-related caption generation, emphasizing that no private information should appear in the captions produced by the VLM captioner. After caption generation, we employ the large language model Llama-3.1-8B [54] to further detect and remove privacy-violating content in the captions. This procedure ensures that all captions, and consequently the generated images, remain privacy-safe. The detailed prompt templates are shown in Table 2.



(a) Gender distribution of the face-related subset. (b) Racial distribution of the face-related subset.

Figure 6: Demographic composition of the real face-related subset. (a) Gender distribution showing the ratio of male and female faces. (b) Racial distribution across six demographic categories.

B Choice of Vision-Language Model (VLM)

In our dataset construction pipeline, we adopt QwenVL-Chat as the captioning model, as it represented a state-of-the-art VLM at the time of our experiments and consistently produced high-quality prompts that satisfied our dataset requirements. To validate this choice, we conducted comparative experiments using several vision-language models (VLMs), as presented in Table 4. The results show that both text and image similarities between the generated prompts and the corresponding images remain consistently high across models, suggesting that the specific choice of VLM has a relatively limited influence on prompt quality. This observation can be attributed to the large-scale and diverse training data used by modern VLMs, which endow them with strong generalization capabilities.

Table 5: Generation parameters of open source models.

Model Name	num_inference_steps	guidance_scale	width/height	enable_model_cpu_offload
SD V1.5 [57]	30	7.5	512	No
SD V2.1 [57]	30	7.5	768	No
SD V3-medium [19]	28	7.0	1024	No
SD V3.5-medium [19]	40	4.5	1024	No
SDXL-base-V1.0 [55]	30	5.0	1024	No
FLUX.1-schnell [41]	4	3.5	512	Yes
Kandinsky-3 [67]	25	4.0	768	Yes
PixArt-XL-2-1024-MS [11]	20	6.0	1024	No
Playground V2.5 [42]	50	3.0	1024	Yes
CogView3-Plus [84]	50	7.0	1024	Yes
HiDream-I1-fast [31]	16	0.0	1024	Yes
Hunyuan-DiT [45]	35	6.0	1024	Yes
Z-Image [65]	9	0.0	1024	Yes
FLUX.2-klein [5]	4	1.0	1024	Yes
GLM-Image [82]	50	1.5	1024	Yes

C Image Generation Details

The dataset construction is conducted on an RTX 3090 GPU with 24 GB of memory. The generation parameters of the open-source models are listed in Table 5.

D Training Details

Training Subset Selection for Semantic Task For the semantic-split task, we select three subsets: “cat,” “bedroom” and “human face” (from FFHQ) as representative subsets for training, based on the following reasons: (1) All semantic classes can be categorized into three broad groups: scenes (including “church,” “bedroom” and “classroom”), animals (including “dog,” “cat” and “wild”), and human faces (including “celebrity face” from CelebA-HQ and “human face” from FFHQ). For each group, we select one subset as its representative. (2) For each group, we choose the most commonly used semantic concept: “bedroom” for scenes, “cat” for animals, and FFHQ “human face” for human faces, as FFHQ offers greater age diversity compared to CelebA-HQ.

Training Settings of Attributors We utilize different training settings for different attributors, as shown below. For any settings not mentioned, the default configuration is applied: training for 10 epochs for the standard task and 15 epochs for the semantic task, using the Adam optimizer with an initial learning rate of 0.001, a batch size of 32, and cross-entropy loss by default.

ResNet50 [30] We use a pretrained model from the Python package torchvision.models as backbone, replacing the classifier with identity and adding a linear layer for classification. The number of training epochs is 20 for standard task.

DCT-CNN¹ [21] We apply the DCT transform to images following the official repository, and use a simple CNN with four convolutional layers as the backbone for attribution.

Cioni et al. [14] We use pretrained CLIP Model² as the backbone. With the backbone frozen, we train a logistic regressor using L2 loss and the LBFGS solver [47], with a maximum of 1000 training iterations.

HiFi-Net³ [28] We utilize NLCDetection and HighResolutionNet from the official repository, designing the multi-level labels as shown in table 6 based on the attributes of generative models (e.g., open source or commercial, DiT, AR, or LDM-based, etc.). The training batch size is set to 8.

Li et al. [43] We reproduce MHF and DEFL based on the paper. Additionally, we employ a neural network classifier and combine dual contrastive loss with cross-entropy loss for model fitting. The batch size is set to 8, and the number of epochs is 10 for both the standard and semantic tasks.

DNA-Det⁴ [77] We adopt the main architecture from the official repository and train for 10 epochs in both the pre-training phase and the attribution training phase for each task.

¹<https://github.com/RUB-SysSec/GANDCTAnalysis/>

²<https://huggingface.co/laion/CLIP-ViT-H-14-laion2B-s32B-b79K>

³https://github.com/CHELSEA234/HiFi_IFDL

⁴<https://github.com/ICTMCG/DNA-Det>

Table 6: Multi level label mapping for HiFi-Net.

Model Name	Level 0	Level 1	Level 2	Level 3
GPT4-o	0	0	0	0
DALL-E 3	0	0	0	11
Gemini-2.0-flash-exp-image-generation	0	0	0	12
Grok3-image	0	0	0	13
Ideogram-generate-V-1-TURBO	0	0	0	16
Kling-image-V1	0	0	0	19
Midjourney V5.2	0	0	0	20
Midjourney V6.0	0	0	0	21
Doubao-Seedream-3.0-t2i	0	0	0	26
Doubao-Seedream-5.0-lite	0	0	0	27
Gemini-2.5-flash-image	0	0	0	28
Gemini-3-pro-image	0	0	0	29
GPT-image-1	0	0	0	30
GPT-image-1.5	0	0	0	31
SD V1.5	0	1	1	6
SD V2.1	0	1	1	7
SD V3-medium	0	1	1	8
SD V3.5-medium	0	1	1	9
SDXL-base-V1.0	0	1	1	10
FLUX.1-schnell	0	1	2	2
Kandinsky-3	0	1	2	3
PixArt-XL-2-1024-MS	0	1	2	4
Playground V2.5	0	1	2	5
FLUX.2-Klein	0	1	2	23
Z-Image	0	1	2	25
CogView3-Plus	0	1	3	1
HiDream-I1-fast	0	1	3	14
Hunyuan-DiT	0	1	3	15
Infinity-2B	0	1	4	17
Janus-Pro	0	1	4	18
GLM-Image	0	1	4	24
real	1	2	5	22

RepMix⁵ [7] We adopt the complete network architecture from the official repository. Notably, we forgo data augmentation in the data processing stage.

PatchForensics⁶ [9] We use Xception as the backbone, which is the default model in the official repository. For the accuracy metric, we select acc_D_voted (where the predicted label is the one with the highest vote count across all patches). The number of epochs is set to 20 for both tasks.

PatchCraft [85] We strictly reproduce the method as described in the paper, with the only modification being the classifier head changed from single-class to multi-class classification.

SSP⁷ [10] We adopt the data processing strategy from the repository to extract the simplest patches and utilize a pretrained ResNet-50 for attribution. Both tasks are trained for 10 epochs each.

GFD [76] We reproduce this method following the paper, employing a U-Net encoder-decoder for fingerprint extraction, a PatchGAN⁸ discriminator and a pretrained ResNet-50 as auxiliary classifier. In each training step,

⁵https://github.com/tubui/image_attribution

⁶<https://github.com/chail/patch-forensics>

⁷<https://github.com/bcmi/SSP-AI-Generated-Image-Detection>

⁸<https://github.com/He-jerry/PatchGAN/blob/master/network.py>

we first train the U-Net fingerprint generator, then jointly train the discriminator and classifier. Batch size is set to 16.

UCF⁹ [75] We adopt the entire network architecture from official repository, modifying only the attribution head and swapping the loss weights between detection and attribution. The number of epochs is set to 10 for both tasks.

FSD¹⁰ [73] We reproduce this method following the few-shot attribution setting in the paper, but use the multiclass implementation in our codebase for unified comparison. Concretely, we adopt an ImageNet-pretrained ResNet-50 backbone, replace the final classification layer with a 1024-dimensional embedding head, and attach a linear attribution classifier for source prediction. We use Adam optimizer with learning rate 1×10^{-4} and a step scheduler with decay factor 0.5 every 5 epochs. The batch size is set to 32, and both the standard balanced-split task and the semantic-split task are trained for 10 epochs each.

Omni-DFA [72] We reproduce this method with a dual-branch ConvNeXt-Small architecture, where one branch processes global views and the other processes local views, and the fused features are projected to a 128-dimensional normalized embedding space for attribution. During training, we maintain learnable class prototypes and a real-image center, and optimize the model using supervised contrastive loss together with a center regularization term for real images. We use AdamW optimizer with learning rate 2×10^{-5} , weight decay 0.01, and a cosine warmup schedule with 2 warmup epochs. The batch size is set to 144, and both the standard balanced-split task and the semantic-split task are trained for 20 epochs each.

E Extended Results and Visualizations

In this section, we present additional result tables, confusion matrices and frequency spectra of generated images.

Results on Three Semantic Tasks Results with accuracy for each degradation level across different attribution methods training on three semantic tasks (i.e., “cat,” “bedroom” and “human face”) are presented in Table 7, Table 8 and Table 9 respectively.

Confusion Matrix We present the confusion matrices for the baseline model ResNet-50 and the best-performing model RepMix, in Figure 7 and Figure 8. While ResNet-50 demonstrates strong performance in standard task, it exhibits relatively poor results in the semantic task, as indicated by the less prominent diagonal in the confusion matrix. In contrast, RepMix displays clear diagonals in both matrices, highlighting its effectiveness in attribution.

Frequency Analysis Following Corvi et al. [15], we extract noise residuals from 1,000 images per generation source and perform a Fourier transform on the average residual to generate the frequency spectrum, as shown in Figure 9. This figure demonstrates that most advanced generation models, including commercial models, cutting-edge DiTs and ARs leave fewer artifacts in the frequency domain compared to earlier GAN models. This indicates that the latest generators synthesize higher-quality images that are indistinguishable from real images, presenting a more challenging scenario for image attribution.

F Representative Image-Caption Pairs

In this section, we display some representative pairs of images and their corresponding captions generated by QwenVL-chat [3], as illustrated in Figure 10 and Figure 11. These figures demonstrate that the captions accurately describe the main objects in the images with precise details, thanks to the tailored prompt template and the exceptional captioning capabilities of QwenVL-chat. The precise captions enable text-to-image generation models to create images that closely adhere to the original in terms of semantic fidelity.

G Additional Visualization of Generated Images

Additional visualizations of generated images will be provided in the supplementary material instead of the appendix.

⁹<https://github.com/SCLBD/DeepfakeBench/>

¹⁰<https://github.com/teheperinko541/Few-Shot-AIGI-Detector>

Table 7: Comparison of different methods training on “Cat.”

Method	Clean Acc. (%)	Degraded Acc.						Avg Acc.
		DS (0.5x)	DS (0.25x)	JPEG (q=65)	JPEG (q=30)	Blur ($\sigma = 3$)	Blur ($\sigma = 5$)	
ResNet-50 [30]	21.9	21.6	20.5	21.8	21.5	17.0	12.3	19.1
DCT-CNN [21]	23.2	19.9	15.3	18.9	16.8	7.8	3.3	13.7
HiFi-Net [28]	50.8	46.6	29.5	17.5	12.7	32.1	10.4	24.8
Li et al. [43]	44.9	39.4	26.2	15.7	14.1	12.8	7.6	19.3
DNA-Det [77]	<u>68.6</u>	60.3	27.2	13.6	11.4	30.0	28.5	28.5
RepMix [7]	66.3	<u>65.1</u>	59.2	65.6	63.1	30.4	18.2	50.3
PatchForensics [9]	69.1	66.6	<u>49.7</u>	14.1	7.3	41.2	16.6	32.6
PatchCraft [85]	44.5	5.0	4.5	22.4	9.7	4.4	4.1	8.4
SSP [10]	61.2	53.7	31.5	12.0	7.1	31.8	13.1	24.9
GFD [76]	45.9	45.0	40.8	<u>45.4</u>	<u>41.9</u>	20.4	10.5	<u>34.0</u>
UCF [75]	16.9	15.9	14.6	16.1	15.1	10.8	8.6	13.5
FSD [73]	35.3	33.1	31.1	30.7	19.3	17.1	10.0	23.6
Omni-DFA [72]	36.5	35.1	27.4	31.0	21.1	<u>32.4</u>	<u>27.5</u>	29.1
Avg	45.0	39.0	29.0	25.0	20.1	22.2	11.6	24.7

Table 8: Comparison of different methods training on “Bedroom.”

Method	Clean Acc. (%)	Degraded Acc.						Avg Acc.
		DS (0.5x)	DS (0.25x)	JPEG (q=65)	JPEG (q=30)	Blur ($\sigma = 3$)	Blur ($\sigma = 5$)	
ResNet-50 [30]	18.0	18.0	16.4	17.3	16.7	10.1	9.0	14.6
DCT-CNN [21]	30.9	26.8	17.8	19.8	17.5	7.3	1.9	15.2
HiFi-Net [28]	61.9	43.6	30.4	28.3	20.0	14.6	7.0	24.0
Li et al. [43]	43.2	37.6	23.0	15.1	12.4	10.3	7.0	17.6
DNA-Det [77]	<u>70.6</u>	63.5	41.1	12.5	13.0	24.9	7.5	27.1
RepMix [7]	66.6	<u>64.8</u>	58.9	63.9	60.9	24.9	<u>19.2</u>	48.8
PatchForensics [9]	73.4	71.1	<u>53.8</u>	14.5	7.8	44.9	18.4	<u>35.1</u>
PatchCraft [85]	39.1	6.0	3.7	14.5	9.0	5.2	4.3	7.1
SSP [10]	61.3	50.8	32.8	12.4	10.1	29.4	9.5	24.2
GFD [76]	43.0	37.5	31.0	<u>39.9</u>	<u>35.8</u>	6.3	3.7	25.7
UCF [75]	17.9	16.4	14.9	15.3	13.7	8.1	6.0	12.4
FSD [73]	34.3	31.1	20.7	31.5	14.1	15.3	9.3	20.3
Omni-DFA [72]	39.5	37.6	25.9	31.5	19.8	<u>34.5</u>	28.4	29.6
Avg	46.7	38.9	28.7	23.7	19.3	16.8	8.6	23.2

Table 9: Comparison of different methods training on “Human Face.”

Method	Clean Acc. (%)	Degraded Acc.						Avg Acc.
		DS (0.5x)	DS (0.25x)	JPEG (q=65)	JPEG (q=30)	Blur ($\sigma = 3$)	Blur ($\sigma = 5$)	
ResNet-50 [30]	26.3	25.9	24.0	26.0	25.5	22.6	16.8	23.5
DCT-CNN [21]	34.0	30.7	20.6	20.9	16.1	5.6	1.4	15.9
HiFi-Net [28]	56.4	47.4	29.6	27.5	18.6	22.4	8.2	25.6
Li et al. [43]	51.1	43.2	25.4	15.4	13.8	13.5	9.7	20.2
DNA-Det [77]	74.6	<u>62.8</u>	30.7	10.2	8.3	37.4	9.1	26.4
RepMix [7]	59.9	58.2	53.7	63.8	60.5	34.5	<u>24.0</u>	49.1
PatchForensics [9]	<u>67.2</u>	64.3	<u>42.0</u>	9.5	5.4	43.3	13.9	29.7
PatchCraft [85]	39.0	5.3	5.4	16.5	11.6	5.0	4.9	8.1
SSP [10]	62.0	54.0	28.9	10.1	7.1	30.2	10.8	23.5
GFD [76]	25.7	22.7	22.7	29.5	31.1	29.2	13.1	22.3
UCF [75]	21.8	21.4	19.5	21.1	19.8	13.8	9.7	17.6
FSD [73]	36.8	35.3	26.2	25.6	15.4	15.9	9.8	21.4
Omni-DFA [72]	43.4	41.5	28.2	<u>39.1</u>	<u>32.8</u>	<u>38.9</u>	33.5	<u>35.7</u>
Avg	45.8	39.4	28.0	24.4	20.3	22.8	12.3	24.5

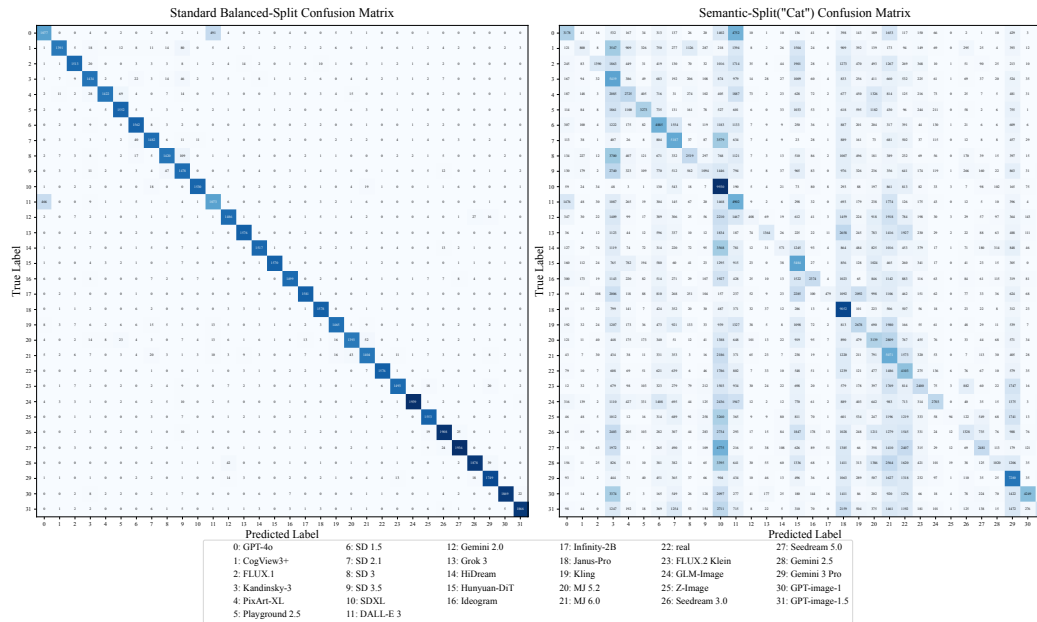


Figure 7: Confusion matrix of ResNet-50.

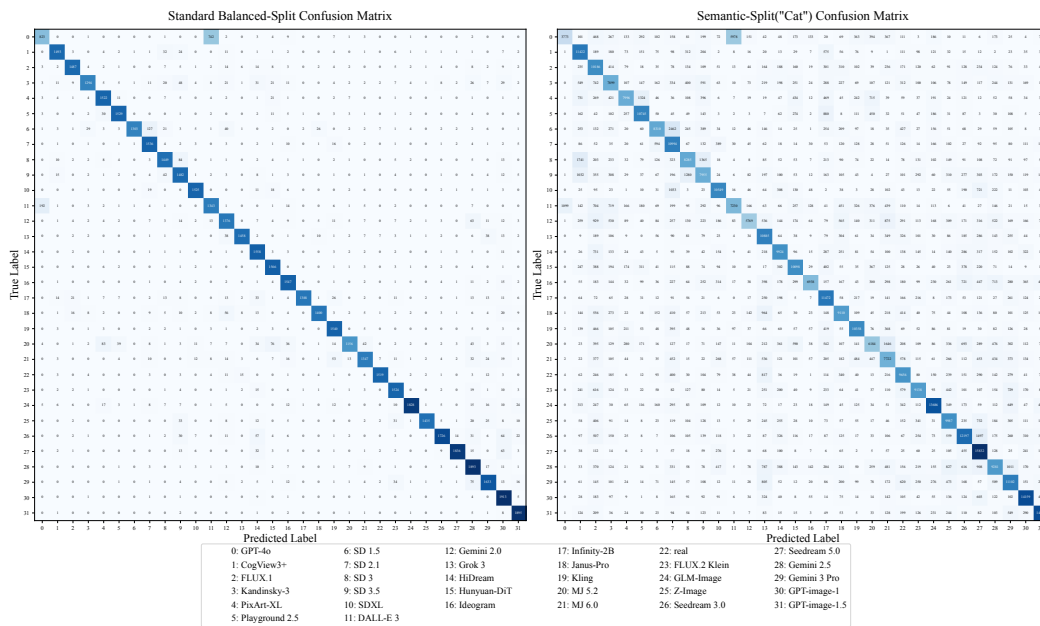


Figure 8: Confusion matrix of RepMix.

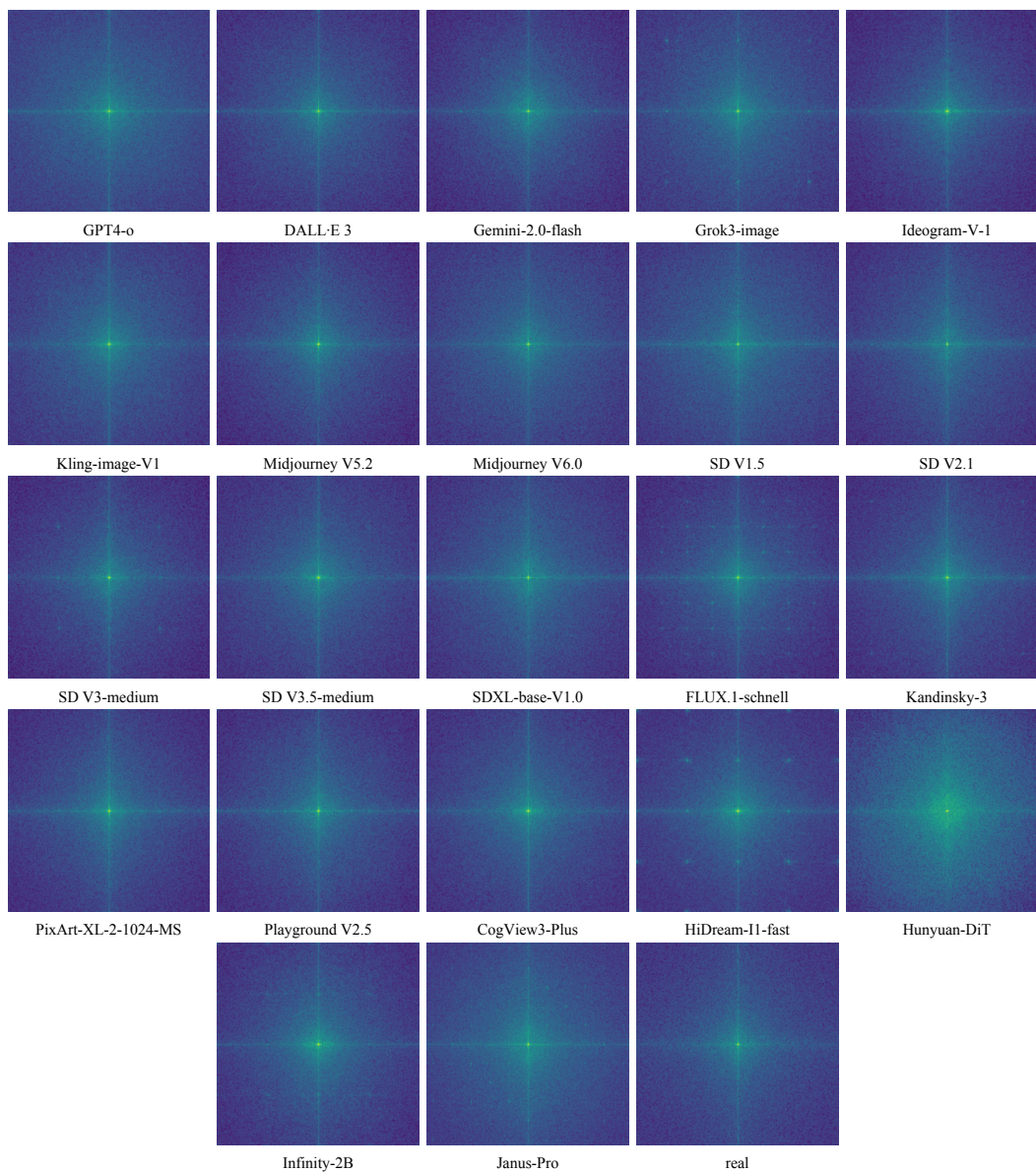


Figure 9: Frequency spectra of generated images from a subset of generation sources.



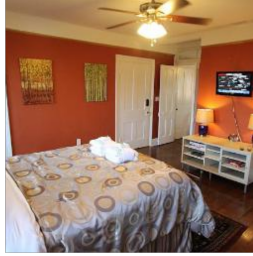
Figure 10: Representative image-caption pairs (upper half).



A cozy bedroom with a large bed, brown furniture, and a wooden ceiling with exposed beams. The room is illuminated by warm lighting, creating a comfortable atmosphere.



A bedroom scene with a large red wardrobe, a bed with pink sheets and two pillows, and a white air conditioner. The room is painted white and has a skylight.



A bedroom scene with a bed, a ceiling fan, a television, a nightstand, and a potted plant. The walls are painted orange, and the room is well-lit.



A cozy bedroom scene with a bed, bookshelf, and comfortable chair. The walls are painted in a warm yellow color, and the room is well-lit, creating a welcoming atmosphere.



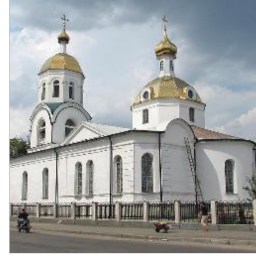
A church scene with a stone building, a path leading to it, and green grass surrounding the area. The colors are muted, and the lighting is dim, creating a serene atmosphere.



A church with a tall steeple and a pointed roof is seen in the distance. The church is surrounded by trees and a red fence. The sky is gray and overcast.



A white church with a tall steeple and a cross on top. The church has a pointed roof and a small porch. The sky is overcast.



A church scene with a white and gold church, a fence surrounding the perimeter, a motorbike parked in front, and a blue sky with clouds in the background.



A classroom scene with students seated at desks, a whiteboard on the wall, and a chalkboard in the background. The walls are painted white, and the lighting is bright.



A classroom with wooden desks and chairs, a blackboard at the front, and a computer on a cart in the back. The room is well-lit with natural light.



A classroom scene with a teacher at the front, surrounded by a blackboard, a computer, and several books. The room features multiple desks and chairs, with bright colors and ample lighting.



A classroom scene with students seated at desks, a chalkboard on the wall, and a flag hanging from the ceiling. The room is painted white and has a bright, well-lit atmosphere.



A coral reef with a variety of colorful fish swimming around. The reef is covered in various types of coral and sea plants. The mood is serene and peaceful.



A dung beetle sits on a leaf in a natural setting. The beetle is black and shiny, with a flat back and large antennae. The mood is serene and peaceful.



A black and silver padlock is attached to a black chain. The chain is wrapped around a white background. The padlock has the word "Raleigh" written on it.



A can of La Rose hair spray is shown with a black background and red rose petals. The label features a rose and the words "La Rose Hair Spray."

Figure 11: Representative image-caption pairs (lower half).